Available online at www.sciencedirect.com
SCIENCE DIRECT®
Nuclear Instruments and Methods in Physics Research A 537 (2005) 637–657
NUCLEAR INSTRUMENTS & METHODS IN PHYSICS RESEARCH Section A
www.elsevier.com/locate/nima

Rare ISotopes INvestigation at GSI (RISING) using gamma-ray spectroscopy at relativistic energies

H.J. Wollersheim[a], D.E. Appelbe[b], A. Banu[a], R. Bassini[c,d], T. Beck[a], F. Becker[a], P. Bednarczyk[a,d,e], K.-H. Behr[a], M.A. Bentley[f], G. Benzoni[c,d], C. Boiano[c,d], U. Bonnes[g], A. Bracco[c,d], S. Brambilla[c,d], A. Brünle[a], A. Bürger[h], K. Burkard[a], P.A. Butler[i], F. Camera[c,d], D. Curien[j], J. Devin[j], P. Doornenbal[a], C. Fahlander[k], K. Fayz[b], H. Geissel[a], J. Gerl[a], M. Górska[a,*], H. Grawe[a], J. Gręboszˊ[a,e], R. Griffiths[b], G. Hammond[f], M. Hellström[a], J. Hoffmann[a], H. Hübel[h], J. Jolie[l], J.V. Kalben[g], M. Kmiecik[e], I. Kojouharov[a], R. Kulessa[m], N. Kurz[a], I. Lazarus[b], J. Li[a,n], J. Leske[h], R. Lozeva[a,o], A. Maj[e], S. Mandal[a], W. Męczyński[e], B. Million[c,d], G. Münzenberg[a], S. Muralithar[p], M. Mutterer[g], P.J. Nolan[i], G. Neyens[q], J. Nyberg[r], W. Prokopowicz[a], V.F.E. Pucknell[b], P. Reiter[l], D. Rudolph[k], N. Saito[a], T.R. Saito[a], D. Seddon[i], H. Schaffner[a], J. Simpson[b], K.-H. Speidel[h], J. Styczeńˊ[e], K. Sümmerer[a], N. Warr[l], H. Weick[a], C. Wheldon[a], O. Wieland[c,d], M. Winkler[a], M. Zięblińˊski[e]

[a]*Gesellschaft für Schwerionenforschung, Planckstrasse 1, D-64291 Darmstadt, Germany*
[b]*CCLRC Daresbury Laboratory, Daresbury Warrington, Cheshire WA4 4AD, United Kingdom*
[c]*Department of Physics, University of Milano, Milano, Italy*
[d]*INFN sez. Milano Via G. Celoria, 16, I-20133 Milano, Italy*
[e]*Niewodniczańˊski Institute of Nuclear Physics, Polish Academy of Sciences, ul. Radzikowskiego 152, 31-342 Krakow, Poland*
[f]*Department of Physics, Keele University, Keele, Staffordshire ST5 5BG, United Kingdom*
[g]*Institut für Kernphysik, TU Darmstadt, Schlossgartenstrasse 9, D-64289 Darmstadt, Germany*
[h]*Helmholtz-Institut für Strahlen- und Kernphysik, Nußallee 14-16, D-53115 Bonn, Germany*
[i]*Department of Physics, University of Liverpool, Liverpool L69 7ZE, United Kingdom*
[j]*IReS, B.P. 28, F-67037 Strasbourg Cedex 2, France*
[k]*Department of Physics, Lund University, Box 118, SE-22100 Lund, Sweden*
[l]*Institut für Kernphysik, Univ. Köln, Zülpicher strasse 77, D-50937 Köln, Germany*
[m]*Nuclear Physics Division, Jagiellonian University, ul. Reymonta 4, 30-059 Krakow, Poland*

*Corresponding author.
E-mail addresses: h.j.wollersheim@gsi.de (H.J. Wollersheim), M.Gorska@gsi.de (M. Górska).

doi:10.1016/j.nima.2004.08.072

[n]Institute of Modern Physics, the Chinese Academy of Science, P.O. Box 31, Lanzhou 730000, China
[o]Faculty of Physics, University of Sofia "St. Kl. Ohridski", 5 J. Bourchier blvd., 1164 Sofia, Bulgaria
[p]Nuclear Science Center, New Delhi 110067, India
[q]Instituut voor Kern-en Stralingsfysica, K.U. Leuven, Celestijnenlaan 200D, B-3001 Leuven,Belgium
[r]Department of Radiation Sciences, Uppsala University, Box 535, SE-75121 Uppsala, Sweden

Received 13 April 2004; received in revised form 29 June 2004; accepted 10 August 2004
Available online 11 September 2004

Abstract

The Rare ISotopes INvestigation at GSI project combines the former EUROBALL Ge-Cluster detectors, the MINIBALL Ge detectors, BaF_2-HECTOR detectors, and the fragment separator at GSI for high-resolution in-beam γ-ray spectroscopy measurements with radioactive beams. These secondary beams produced at relativistic energies are used for Coulomb excitation or secondary fragmentation experiments in order to explore the nuclear structure of the projectiles or projectile like nuclei by measuring de-excitation photons. The newly designed detector array is described and the performance characteristics are given. Moreover, particularities of the experimental technique are discussed.

PACS: 13.40.Hq; 13.40.−f; 25.60.−t; 25.70.Mn; 25.75.−q; 29.30.Kv

Keywords: Radioactive beams; Relativistic heavy-ion beams; Electromagnetic interaction; Fragmentation reaction; Projectile excitation; γ-ray spectroscopy

1. Introduction

The SIS/FRS facility [1] at GSI provides secondary beams of unstable rare isotopes produced via fragmentation reactions or fission of relativistic heavy ions. Many of these unique radioactive beams have sufficient intensity to enable in-beam γ-ray spectroscopy measurements. In the first Rare ISotopes INvestigation at GSI (RISING) experiments such beams are being exploited at an energy of 100 A MeV to perform relativistic Coulomb excitation of radioactive projectiles and secondary nuclear reactions such as nucleon removal and fragmentation. The RISING set-up is optimised for the investigation of key subjects of nuclear structure research, namely:

- shell structure of known and predicted doubly magic nuclei and nuclei in their vicinity far off stability;
- isospin symmetry along the N = Z line and mixed symmetry states;
- deformed shapes and shape coexistence;
- collective modes of nuclear excitation and E1 strength distribution.

High resolution γ-ray spectroscopy at relativistic beam energies is an experimental challenge. Limitations imposed by large Doppler effects and background caused by atomic processes and unwanted nuclear interactions have to be considered. Both the incoming and outgoing particles of the secondary target have to be identified in mass and charge and their energy and direction determined. The design of the germanium detector array and the heavy-ion tracking detectors were optimised to achieve the highest possible efficiency, energy resolution, and position resolution for heavy ions. In this paper, the experimental set-up for RISING experiments at beam energies of $\sim$ 100 A MeV is described. The performance of the components and first results of Coulomb excitation and secondary fragmentation measurements are presented.

2. Atomic and nuclear processes at relativistic energies

2.1. Angular and energy-loss straggling

In relativistic heavy-ion reactions with secondary beams, thick targets can be used which partially compensate for the low beam intensity. The slowing-down of the fragments in the target layer contributes to the kinematics and results in an energy distribution. The distribution is further enlarged by multiple scattering in the target introducing angular straggling. Fig. 1 depicts the angular straggling [2,3] in a gold target for Ni, Sn and Pb projectiles at 100 A MeV as a function of the target thickness.

While the energy-loss straggling at relativistic energies is small ($<1\%$) even for relatively thick targets (600 mg/cm^2), the angular straggling shows a strong dependence on target thickness, which limits the impact parameter measurement for peripheral collisions.

2.2. Atomic background radiation

Atomic processes are the main source of background γ radiation in relativistic heavy-ion reactions. The main atomic processes contributing to this background are [4–6], (i) K and L shell X-rays from ionised target atoms, (ii) radiative electron capture (REC) of the target electrons into the projectile K and/or L shells, (iii) primary bremsstrahlung (PB) from target electrons produced by the collisions with the projectile, (iv) secondary bremsstrahlung (SEB) from energetic knock-out electrons re-scattering in the target and/or the surrounding material. The atomic cross-sections of all these processes depend strongly on the atomic number of the projectile and target. Based on experimental results, the double-differential cross-section $d^2\sigma/dE\,d\Omega$ of the four atomic processes given above can be calculated empirically [6]. The angle-integrated cross-section $d\sigma/dE$ is illustrated in Fig. 2 for ^{132}Sn fragments at different beam energies (left) and on Be, Sn and Au targets (right).

For small γ-ray energies the angle-integrated cross-section can reach several kb/keV, which is at least 4 orders of magnitude larger than typical Coulomb excitation and nuclear reaction cross-sections. To perform nuclear structure γ-ray spectroscopy (especially Coulomb excitation with heavy targets) down to 400 keV, the beam energy has to be limited to 100 A MeV. This energy of 100 A MeV will be fixed for the following discussion and is a basic quantity for the design of the Ge-Cluster detector array in RISING.

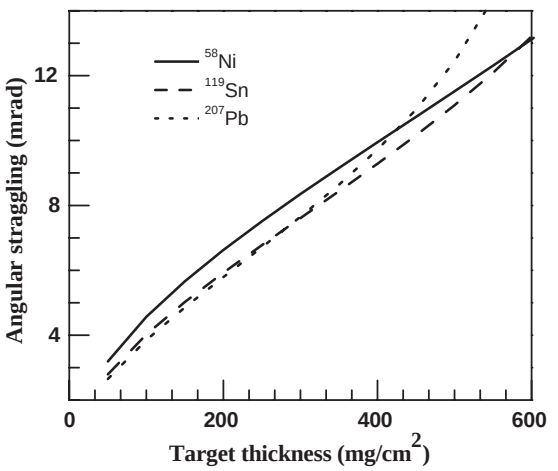

Fig. 1. Angular straggling (σ) in a gold target as a function of the target thickness for Ni (solid line), Sn (long-dashed line) and Pb projectiles (short-dashed line) at 100 A MeV.

2.3. Coulomb excitation at 100 A MeV

Coulomb excitation at a relativistic energy of 100 A MeV is a powerful spectroscopic method to study low-lying collective states of exotic nuclei produced at fast-beam facilities (for review see Ref. [7] and references therein). It takes advantage of the large beam velocities and allows the use of thick secondary targets (in the range of hundreds of mg/cm^2). Contributions to the excitation process by the nuclear force are excluded by selecting reactions at an extremely forward scattering angle, corresponding to a large impact parameter.

An important parameter for this measurement is the grazing angle and the distance of closest approach $D = R_{\mathrm{int}}$ at the nuclear interaction radius. For the present discussion we refer to the

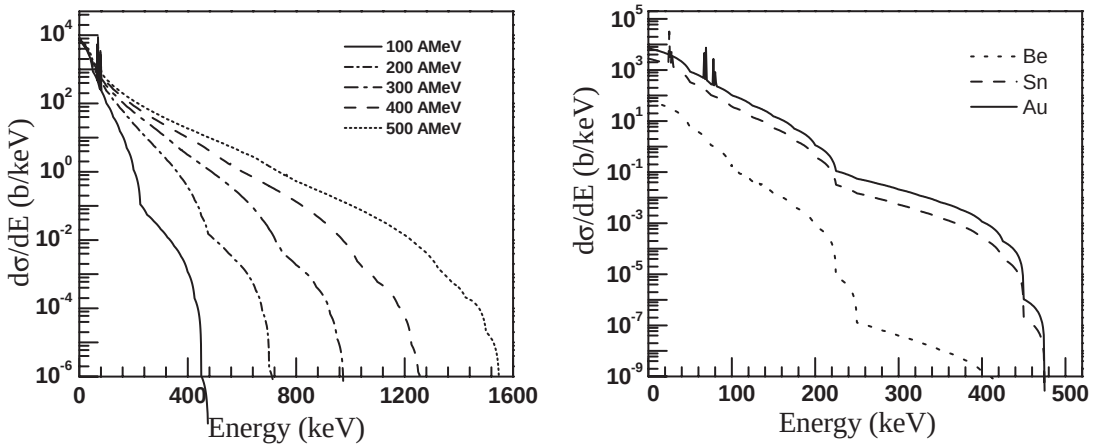

Fig. 2. Angle-integrated cross-section as a function of γ-ray energy for the atomic γ-ray background from ^{132}Sn on a Au target at different beam energies (left). The cross-section dependence on different target materials (Be, Sn, Au) for ^{132}Sn fragments at 100 A MeV (right).

definition of R_{int} following Wilcke et al. [8]:

$$R_{\mathrm{int}} = C_{\mathrm{p}} + C_{\mathrm{t}} + 4.49 - \frac{C_{\mathrm{p}} + C_{\mathrm{t}}}{6.35} \quad \text{(fm)}$$

$$C = R(1 - 1/R^2)$$

$$R = 1.28A^{1/3} - 0.76 + 0.8A^{-1/3}$$

with the nuclear radius R for a homogeneous (sharp) mass distribution, the nuclear radius C for a diffuse Fermi mass distribution and the mass number, A, for the projectile, p, and target nucleus, t, respectively. For the beam-target combination ^{84}Kr + ^{197}Au the nuclear interaction radius is $R_{\mathrm{int}} = 14.2$ fm.

For small deflections ($\sin\theta \simeq \tan\theta \simeq \theta$) and including relativistic effects we obtain for the scattering angle ϑ in the laboratory frame [9]

$$\vartheta \simeq \frac{2Z_{\mathrm{p}}Z_{\mathrm{t}}e^2}{m_0c^2\gamma\beta^2 b} = \frac{2.88Z_{\mathrm{p}}Z_{\mathrm{t}}[931.5 + T_{\mathrm{lab}}]}{A_{\mathrm{p}}[T_{\mathrm{lab}}^2 + 1863T_{\mathrm{lab}}]}\frac{1}{b} \quad \text{(rad)}$$

where T_{lab} is the laboratory beam energy in A MeV, b the impact parameter in fm, m_0 the rest mass of the projectile, γ the Lorentz contraction factor, and β the beam velocity in units of velocity of light. Since the scattering for $T_{\mathrm{lab}} = 100$ A MeV is confined to rather small angles, the projectile moves on a straight-line trajectory and the impact parameter b can be replaced by the distance of closest approach D. In this way we can calculate the grazing angle $\vartheta_{\mathrm{gr}}(b = R_{\mathrm{int}})$ which is the largest scattering angle in a Coulomb excitation experiment at relativistic energies.

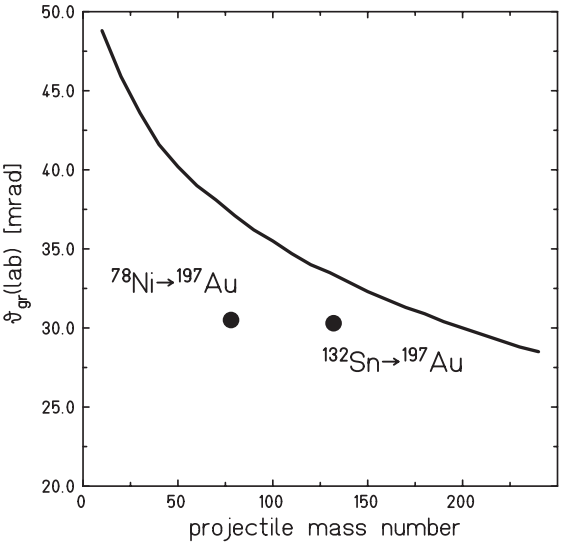

Fig. 3. The grazing angle ϑ_{gr}(lab) is displayed as a function of the projectile mass number for scattering on a ^{197}Au target. The solid line corresponds to projectiles in the valley of stability.

In Fig. 3 the grazing angle ϑ_{gr} is displayed as a function of the projectile mass number for scattering on a ^{197}Au target. For all projectile –

target combinations an angular range of about 3° (52 mrad) is important for Coulomb excitation.

2.4. Fragmentation reactions at the secondary target

Fragmentation reactions at the secondary target are powerful tools for producing exotic nuclear isotopes in excited states see e.g. Refs. [10–12]. Contrary to Coulomb excitation, states with higher spin transfer are populated. The latter can be described with the abrasion–ablation model using the Monte Carlo code ABRABLA [13], or by a simple analytical formula [14]. The average angular momentum calculated with both models is in qualitative agreement with the experimentally observed value.

Besides being an excellent tool for investigating radioactive fragments up to medium spin $4-10\,\hbar$, fragmentation reactions provide a selective trigger, in particular suppressing the huge background from atomic processes.

If the fragmentation cross-section for the isotope of interest is large compared to the competing cross-sections of other channels, this channel could be used directly. However, in most cases the fraction of the isotope in question is too small to be selectable within all isotopes produced. Moreover, even if the selectivity was sufficient, the γ-ray rate limitation would demand a rather low primary beam intensity and, hence, low yield of the reaction channel of interest. Therefore, an intermediate fragment is produced and selected by the FRS, which is directed to the secondary target to yield, in a secondary fragmentation step, the isotope of interest. The intermediate fragment is chosen with respect to its available intensity on one hand and the subsequent production cross-section and relative abundance in the produced isotope cocktail on the other hand. Another criterion is that the population of higher spin states requires more massive fragmentation processes. This optimisation is done by the above-mentioned EPAX calculations [15,16].

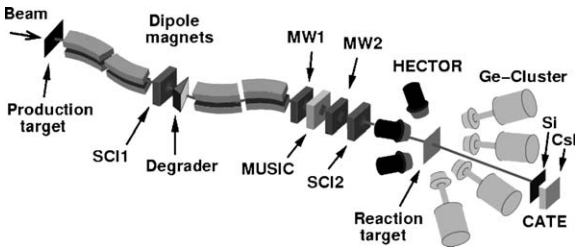

Fig. 4. Schematic layout of the RISING set-up at the FRS. The beam diagnostic elements consist of two multiwire detectors (MW1 and MW2), an ionisation chamber (MUSIC) and two scintillation detectors (SCI1 and SCI2). The γ rays are measured with BaF_2-HECTOR and Ge-Cluster detectors. The ions emerging from the reaction target are identified with the CATE array.

3. Rare isotope beam production, selection, and identification

3.1. Primary beam and target

At SIS/FRS secondary beams of radioactive nuclei are produced by fragmentation of a stable primary beam or fission of a ^{238}U beam on a ^{9}Be or ^{208}Pb target (with typical thicknesses of 1–4 g/cm^2) placed at the entrance of the fragment separator (FRS) (see Fig. 4). Typically, the primary beam energy ranges from 400 to 1000 A MeV for good optical transmission and minimum atomic charge state distribution (i.e. one charge state dominating). The present maximum beam intensity from the SIS synchrotron is $\sim 10^9$/s for medium heavy nuclei (e.g. ^{129}Xe) and $\sim 2\times10^8$/s for ^{238}U. The intensity of particular secondary beam species can be calculated from the luminosity and the production cross-section. For fragmentation reactions the production cross-sections and momentum distributions of the reaction products are rather well known [15,17,18]. The cross-sections are taken from the EPAX parametrisation [15,16], while experimental data are available for nuclear and electromagnetic fission yields [19–25].

3.2. Secondary beam selection

The FRS [1] is a zero-degree magnetic spectrometer and consists of four dipole stages and an

aluminium degrader at the intermediate focal plane, which provides high-energy, spatially separated isotopically pure exotic beams of all elements up to uranium. The nuclei of interest are selected via their magnetic rigidity, $B\rho$, and energy loss, ΔE, in the degrader, the so-called $B\rho$–ΔE–$B\rho$ method [1]. A specific property of the RISING experiments is the use of rather low beam energies (~ 100 A MeV) at the secondary target, which deteriorates the beam quality and transmission through the FRS due to large angular and energy loss straggling in the target and degrader. To simulate the experimental set-up and estimate the properties of the secondary beam with respect to luminosity, separation quality, implantation profiles, and transmission, the simulation programmes MOCADI [26] and LISE++ [27] were used. An example, calculated with MOCADI code, illustrates a radioactive beam quality dependence on its energy. A ^{56}Cr fragment impinging with 313 A MeV on the secondary target has 32% transmission through the FRS, a relative energy resolution, $\Delta E/E$, of 3.4%, and the horizontal beam size amounts to 2.1 cm (FWHM). By slowing down to 136 A MeV, the transmission is reduced to 19%, the relative energy resolution yields $\Delta E/E = 5.0\%$, and the horizontal beam size increases to 3.5 cm (FWHM). A comparison between simulation and measurement is shown in Fig. 5. The basic ion identification is given by plotting the atomic number Z versus A/Q (as the majority of light ions are fully stripped of electrons at ~ 100 A MeV, the measured Q represents Z of the ions). However, the ion identification procedure depends on the selected region of the nuclear chart. To get an optimum identification a more sophisticated analysis of correlations among the measured parameters such as TOF, energy loss and beam position is usually applied.

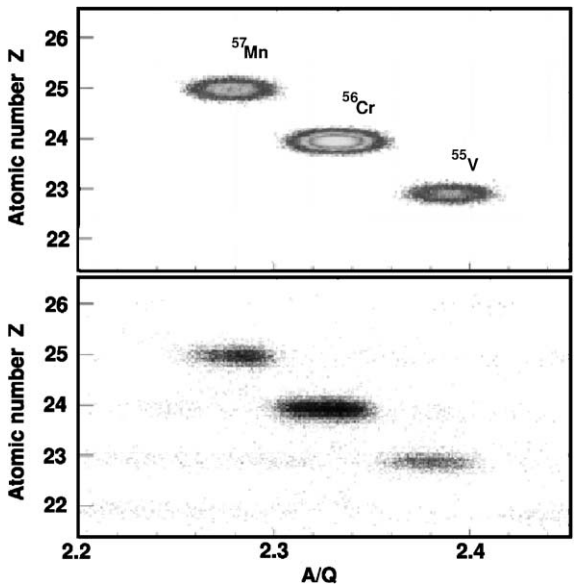

Fig. 5. Comparison of the calculations performed with the LISE++ code (top) with the experimental data (bottom) for the ^{56}Cr setting at a count rate of 10^4/s at SCI1. Plotting the intensity distribution of the atomic number Z versus A/Q gives an identification of the different ions.

3.3. Description of beam detectors, their location and performance

Various types of detectors were used to perform an A and Z identification of the secondary beam ions, including position tracking (see Fig. 4).

Two position-sensitive plastic scintillators (SCI1 and SCI2) were placed at the intermediate and close to the final focal planes providing time of flight (TOF) and position information. The location of the scintillator SCI2 was -1512 mm (upstream) from the target. The scintillation detectors with a thickness of 0.5 mm and a diameter of 250 mm have a typical intrinsic time resolution of about 100 ps (FWHM) [1]. Two Multi-Wire proportional chambers (MW1 and MW2) at -3251 and -2429 mm, respectively, provide the beam position and tracking information. The MW detectors have an active area of 200×200 mm^2 and operate with a mixture of Argon–CO_2 gas at the atmospheric pressure. Therefore thin Capton windows could be used. The readout of the wires representing the x and y planes is performed by the delay-line technique. The position resolution of the MW detectors is below 1 mm [28]. The TOF and $B\rho$ were used to determine the mass-to-charge ratio (A/Q).

The atomic number Z of the secondary beam nuclei is deduced by measuring their energy loss in a MUltiple Sampling Ionisation Chamber (MUSIC) [29] positioned at -2801 mm in front of the

target. The MUSIC consists of eight anode strips covering an active area of $200 \times 80\,mm^2$. The counting gas is CF_4 at the atmospheric pressure. Since the number of electrons generated in the gas are proportional to the square of the charge of the penetrating ion, the signal gives a measure of the atomic number Z of this ion. In addition, the TOF was used to obtain a velocity correction for the Z determination.

Since the secondary beam nuclei are slowed down in the FRS and the subsequent tracking detectors to about 100 A MeV before reaching the secondary target, the fragment identification is worse. While e.g. TOF resolution of 270 ps and a mass resolution of $\Delta A = 0.27$ (FWHM) could be reached during the calibration of the FRS with a stable ^{86}Kr at 419 A MeV, these numbers were increased significantly for the secondary nuclear beams. In addition, the TOF and the mass resolution are intensity dependent, such that for the ^{56}Cr beam a TOF resolution of 2.2 and 3.7 ns (FWHM) could be achieved at the counting rate of 10^4 and 10^6/s, respectively. The corresponding values of mass resolution are 0.59 and 0.89 (FWHM), respectively. For a unique mass identification the latter value therefore determines the count rate limit of SCI1. The identification of the atomic number Z was performed with the MUSIC detector. For the primary ^{86}Kr beam a Z resolution of $\Delta Z = 0.27$ (FWHM), while for the ^{56}Cr beam $\Delta Z = 0.24$ and 0.43 was obtained for the above-mentioned low and high count rates at SCI1, respectively.

4. Reaction channel determination with the CAlorimeter TElescope CATE

Following the reaction on a secondary target at the final FRS focal plane, the scattered particles and breakup products need to be identified in terms of A and Z, and the scattering angle has to be measured. The standard $B\rho$-TOF method for mass determination was not applicable for RISING, since the available space in the experimental area was not sufficient for placing a big magnet. Moreover, the broad charge state distribution of the heavy ions behind the secondary target would impede the mass determination. Therefore, a position-sensitive ΔE–E calorimeter was chosen. The required particle detector should be as efficient as possible and needs to accept the full available secondary beam intensity as it covers zero degree angle. Different beam particle detector designs have been used in the past and the latest generation devices are ΔE–E telescope systems. Energy loss is measured with thin position-sensitive Si detectors, whereas the residual-energy detectors are usually made of CsI(Tl) scintillators [30].

For the RISING project the CAlorimeter TElescope (CATE) array was designed [31] and consists of 3×3 modular ΔE–E telescopes covering the relevant opening angle of 58 mrad (see Section 2.3) at $+1426$ mm from the target and mounted in vacuum. Two types of transmission (ΔE) Si detectors were produced by the company EURISYS and CANBERRA (model: IPP 2D 50×50-300-SPE and PF-50×50-300EB, respectively). The detectors are position sensitive, which can be exploited for the impact parameter measurements in Coulomb excitation. The geometrical size and the active area of each 300 μm thick Si detector was 54×54 and $50 \times 50\,mm^2$, respectively, resulting in a geometrical efficiency of 92%. The central detector is positioned 3 mm behind the plane of the other eight Si detectors.

The energy deposition in the detector array was measured with the back contact, while a resistive layer (sheet resistance 2 kΩ) on the front side of each detector module served as a charge divider to the four corner contacts. The position of an incident ion was determined comparing relative heights of the four signals following a simple geometrical algorithm. Each corner contact is terminated by a 1 kΩ resistor to reduce non-linearities in the position determination as described, e.g. in Ref. [32]. The detector signals are integrated by charge-sensitive preamplifiers (model: CSTA2 made by the Institute of Nuclear Physics, Technical University, Darmstadt [33]). The Si detector prototype energy resolution, obtained with stopped α particles, was 80 keV for the 5.48 MeV ^{241}Am line. Additional tests with heavy ions of about 5 A MeV energy revealed a position resolution of <7 mm (FWHM) [34,35].

The CsI(Tl) detectors provided by the company SCIONIX (model: V502P25/18-E2-Cs-X SSX848) were mounted 40 mm behind the Si array. Each detector has a flat front face of $54 \times 54\,mm^2$ size, a thickness of 10–20 mm and a trapezoidal back shape. The thickness of detectors is sufficient to stop heavy ions with $Z \geqslant 7$ at 100 A MeV and with $Z \geqslant 28$ at 400 A MeV. This covers all possible secondary reaction products expected from the proposed RISING experiments. The detectors were mounted in an aluminium frame of 4 mm thickness between each two neighbours thus yielding the same geometrical efficiency of 92% as for the Si array. The scintillation light of each crystal is collected by a photo diode of $18 \times 18\,mm^2$ size mounted on the trapezoidal back side of the crystal. The signal of the PIN diode was amplified by integrated preamplifiers [36] and yields the residual energy of the fragments after passing through the Si detectors.

Several detector tests using relativistic heavy ions were performed to optimise the final design of the ΔE–E telescopes [35]. A ^{124}Sn beam of 450 A MeV gave values of ΔE corresponding to the resolution of $\Delta Z = 0.7$ (FWHM) for the Si detector. For the same detector a 5 mm (FWHM) position resolution was found in the measurement of the 400 A MeV ^{238}U beam. The CsI(Tl) test detector revealed an energy resolution of 1.0% for a ^{132}Xe beam. Considering the energy spread of the detected beam nuclei and applying a position-dependent energy correction, an intrinsic energy resolution of $\Delta E/E_{res} \approx 0.5\%$ is deduced. The latter correction accounts for the position dependence of the scintillation light production and collection in the detectors.

The CATE array with its nine ΔE–E_{res} telescopes was used in the first RISING experiments at $\sim$ 100 A MeV. Results from a fragmentation reaction and a Coulomb excitation experiment are displayed in Fig. 6. The two-dimensional ΔE–E_{res} plots of one telescope for ^{9}Be(^{55}Ni,xn,yp) and ^{197}Au(^{112}Sn,xn,yp) channels demonstrate the excellent Z resolution. The data were taken under the condition of a particle–γ coincidence. With this requirement one should note that for ^{55}Ni on ^{9}Be all reaction channels are almost equally populated, while for ^{112}Sn on ^{197}Au the inelastic (Coulomb excitation) channel dominates. The extracted Z resolution was 0.7 (FWHM) for the reaction with ^{55}Ni and 0.8 (FWHM) for the ^{112}Sn (a product of ^{124}Xe fragmentation) induced reactions. For the mass identification, which is the subject of a forthcoming paper [31], the combined $\Delta E + E$ information is used to extract from the total kinetic energy the mass number, thereby assuming the same velocity for all reaction products with a given charge.

In the RISING experiments, the accuracy of the position determination, measured with the Si detectors, is limited by the angular spread of the ions after the secondary target. It amounts at least

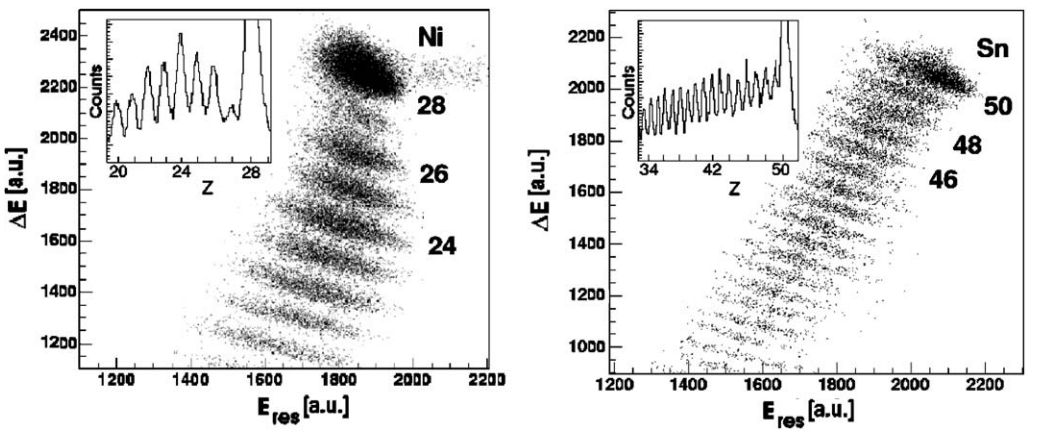

Fig. 6. Two-dimensional ΔE–E_{res} spectra from two RISING experiments exploring ^{9}Be(^{55}Ni,xn,yp) (left) and ^{197}Au(^{112}Sn,xn,yp) (right) reaction. The insets show the extracted element distribution.

to 7 mrad (FWHM)(see Fig. 1) corresponding to a circle of 20 mm diameter at the CATE position. This is large compared to the intrinsic position resolution. Beam intensities of several thousand ions per second could be accepted for the ΔE–E telescopes without deteriorating the detection characteristics. After an accumulated dose of $>10^9$ heavy ions on the central Si detector, the leakage current increased from originally 100 nA to 2 μA. Although the detector resolution did not deteriorate significantly, the detector was replaced at that stage.

5. High-resolution γ-ray detection with Ge-detectors

5.1. Doppler effect at relativistic energies

In the following section we will summarise the relevant formulas [37,38] for the Doppler effect, which are important for the design of the γ-detection array, since the photons from the excited projectiles are emitted in flight. Due to the large beam velocity of $\beta \geqslant 0.4$ at an energy around 100 A MeV, the observed γ-ray energies, E_γ, are strongly Doppler shifted relative to the de-excitation γ-ray energy, $E_{\gamma 0}$, for the projectile at rest according to the following formula:

$$\frac{E_\gamma}{E_{\gamma 0}} = \frac{\sqrt{1-\beta^2}}{1-\beta\cos\vartheta_\gamma}$$

with

$$\beta = \frac{\sqrt{(T_{\mathrm{lab}}/A_{\mathrm{p}})^2 + 1863(T_{\mathrm{lab}}/A_{\mathrm{p}})}}{931.5 + T_{\mathrm{lab}}/A_{\mathrm{p}}}.$$

Fig. 7 shows the Doppler shift for beam energies of 100 and 200 A MeV compared with an energy close to the Coulomb barrier, 6 A MeV. The quantity ϑ_γ denotes the angle between the γ ray and the projectile fragment in the laboratory frame. The small scattering angles of the fast moving projectile fragments ($\vartheta \leqslant 3^\circ$), means we can take the angle ϑ_γ as the γ-ray detection angle with respect to the beam axis in order to simplify the calculation. This approximation will be taken in the following discussion. At $\vartheta_\gamma = 0^\circ$ the γ-ray energy can reach $E_\gamma \approx 1.6E_{\gamma 0}$, while at $\vartheta_\gamma = 180^\circ$ $E_\gamma \approx 0.6E_{\gamma 0}$ for 100 A MeV beam energy.

To find the optimal positions for the γ-detectors, we also have to take the Lorentz boost of the γ

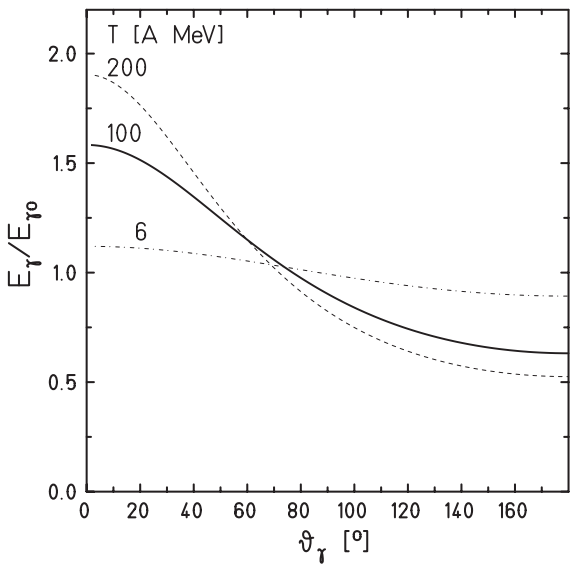

Fig. 7. The ratio of the photon energy E_γ measured in the laboratory frame, to the photon energy $E_{\gamma 0}$ in the rest frame of the projectile versus the laboratory angle ϑ_γ for bombarding energies of 6, 100 and 200 A MeV.

rays into consideration. Since in both laboratory and rest frame the z-axis is the beam direction, we obtain the following relations between the γ-ray emission angle and the solid angle:

$$\phi_\gamma^{\mathrm{rest}} = \varphi_\gamma^{\mathrm{lab}}$$

$$\cos\,\theta_\gamma^{\mathrm{rest}} = \frac{\cos\vartheta_\gamma - \beta}{1-\beta\cos\vartheta_\gamma}$$

$$\frac{\mathrm{d}\Omega_{\mathrm{rest}}}{\mathrm{d}\Omega} = \left(\frac{E_\gamma}{E_{\gamma 0}}\right)^2 = \frac{1-\beta^2}{(1-\beta\cos\vartheta_\gamma)^2}.$$

One should note that the relation between the solid angles is given by the square of the Doppler shift (see Fig. 7). This leads to a γ-ray intensity distribution which is peaked at forward angles and, hence, increases the γ-detection efficiency at small angles.

To correct for the Doppler shift, i.e. to get the γ-transition energy $E_{\gamma 0}$ from the detected E_γ, β and ϑ_γ must be determined precisely. The velocity, β, can usually be derived with an accuracy of better than 1% (TOF measurement), but the accuracy of ϑ_γ is worse in most cases because of the opening angle of standard γ-ray detectors. The Doppler broadening due to the opening angle is given by

$$\frac{\Delta E_{\gamma 0}}{E_{\gamma 0}} = \frac{\beta\,\sin\,\vartheta_\gamma}{1-\beta\cos\,\vartheta_\gamma}\Delta\vartheta_\gamma$$

where the opening angle can be estimated by

$$\Delta\vartheta_\gamma = 0.622\,\arctan\frac{d}{R+30}.$$

Here d(mm) denotes the diameter of the Ge crystal, R(mm) the distance to the target, 30 mm is the assumed interaction depth in a Ge crystal and the factor 0.622 which was determined empirically allows the calculation of the FWHM value. For the case of $d = 59$ mm (for crystals of a Cluster detector), $R = 700$ mm we obtain an opening angle of $\Delta\vartheta_\gamma = 2.9^\circ$ or 50 mrad and an energy resolution $\Delta E_{\gamma 0}/E_{\gamma 0} = 1\%$ (for $\beta = 0.43$) at a detection angle of $\vartheta_\gamma = 15^\circ$. Fig. 8 (left) shows the Doppler broadening for an opening angle of $\Delta\vartheta_\gamma = 3^\circ$ versus the laboratory angle ϑ_γ.

For very short-lived states in the pico-second range the expected γ-ray energy resolution $\Delta E_{\gamma 0}/E_{\gamma 0}$ depends also on the projectile velocity β. Since rather thick targets are used, the projectiles may decay within the target during the slowing down process. Therefore, the velocity of the projectile at the time of γ-ray emission is not known precisely. The relevant formula for the Doppler broadening is given below

$$\frac{\Delta E_{\gamma 0}}{E_{\gamma 0}} = \frac{\beta-\cos\,\vartheta_\gamma}{(1-\beta^2)(1-\beta\,\cos\,\vartheta_\gamma)}\,\Delta\beta.$$

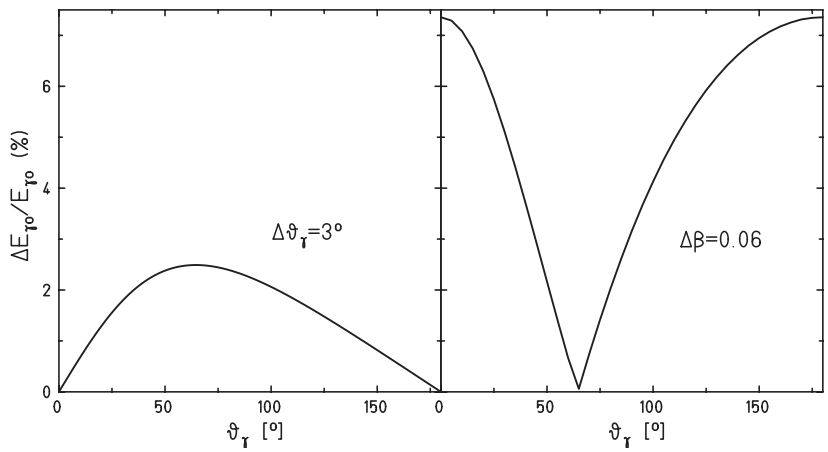

Fig. 8. The expected γ-ray energy resolution $\Delta E_{\gamma 0}/E_{\gamma 0}$ as a function of the laboratory angle ϑ_γ for a bombarding energy of 100 A MeV. For the Doppler broadening an opening angle of $\Delta\vartheta_\gamma = 3^\circ$ (left) and a spread in the beam velocity of $\Delta\beta = 6\%$ is assumed (right), respectively.

Fig. 8(right) shows an example of the Doppler broadening for a spread in the beam velocity of $\Delta\beta = 6\%$ versus the laboratory angle ϑ_γ.

In typical Coulomb excitation experiments, Au targets with a thickness of 400 mg/cm^2 are used. If we consider a fragment beam (100 A MeV) and a mean lifetime for a state of $\tau = 0.5$ ps, approximately 70% of the excited projectiles will decay within the target. The uncertainty in the beam velocity is $\Delta\beta = 6\%$ which effects the γ-ray energy resolution especially at forward and backward angles. Therefore, we have to consider effects on the γ-ray line shape due to energy losses of the excited nuclei in the target. For the example mentioned above, the mean lifetime $\tau = 0.5$ ps will not prevent the observation of the γ-ray transition, since $\approx 30\%$ of the γ-ray intensity remains in the sharp component of the γ-peak ($\Delta E_{\gamma 0}/E_{\gamma 0} = 1\%$).

5.2. Cluster array for experiments at relativistic energies

The γ-ray detectors used in the RISING experiment are the Cluster Ge detectors from the EUROBALL spectrometer [39] and the segmented Ge detectors from the MINIBALL spectrometer [40].

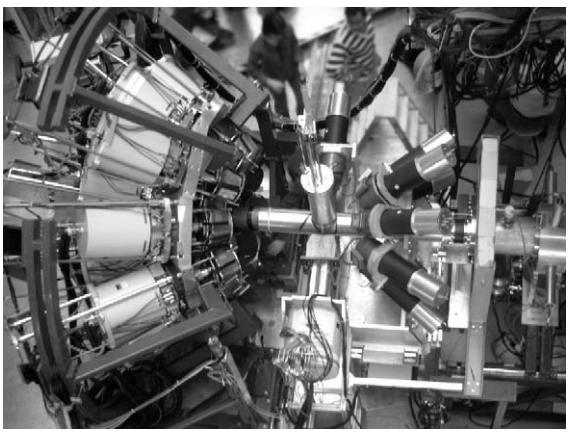

Fig. 9. A photograph of the set-up of the first phase of RISING. The beam comes from the right. BaF_2-HECTOR array, target chamber with one BaF_2 and one VEGA monitor detectors placed perpendicular to the beam axis, and the Ge-Cluster array are shown on the right, middle, and left, respectively.

In the first phase of the project the array was made up of 15 Cluster detectors. The photograph of the set-up is shown in Fig. 9. Each Cluster detector comprises seven closely packed tapered hexagonal Ge crystals [41] housed in a common cryostat. Each Ge crystal is encapsulated in a permanently sealed Al can. Due to the possibility to add back the energies measured in neighbouring crystals after Compton scattering a high full-energy efficiency is maintained up to γ-ray energies of several MeV [42]. Therefore, Cluster detectors are ideally suited for the fast beam RISING experiments where γ-ray energies are strongly Doppler shifted to higher energies.

For experiments with beam energies around 100 A MeV the Ge detectors have to be positioned at forward angles in order to maximise the effective solid angle affected by the Lorentz boost, and to minimise the Doppler broadening effect (see previous section). For optimum packing the crystals are arranged in three rings around the beam pipe, with the axis of the central detectors in each ring positioned at 15°, 33°, and 36°.

A design goal for the array was to obtain about 1% energy resolution for a γ transition, emitted from a nucleus moving at $\beta = 0.43$. This criterion defines the distance to the target.

Due to the Lorentz boost the main efficiency contribution comes from the detectors closest to the beam line in the forward direction. Using the formula given in Section 5.1, the efficiency and resolution of the detectors was estimated based on the known performance of the detectors at 445 mm (regular distance in EUROBALL spectrometer), using standard γ-ray sources ($\beta = 0$). At 15° a distance of 700 mm to the target was obtained. The mechanical constraint of the 16 cm diameter beam pipe defined this to be the most forward angle possible. In addition, due to the complexity of the downstream CATE detector, the distance of this first ring from the target could not be changed.

The resolution of the detectors in the 2nd and 3rd rings at a distance of 700 mm, at $\beta = 0.43$, would be significantly worse. Therefore, the array was designed such that these detectors could be positioned at a variable distance from the target (700–1400 mm). This various detector configurations to be chosen depending on the relative

Table 1
Detectors and their positions in the RISING γ-ray spectrometer

Ring	Detector type	Number	Angle (deg)	Distance (mm)
1	Cluster	5	15.9	700
2	Cluster	5	33.0	700–1400
3	Cluster	5	36.0	700–1400
4	MINIBALL	4	51.3	180–500
	MINIBALL	1	51.3	227–500
5	MINIBALL	2	86.0	180–500
	MINIBALL	1	86.0	232–500

The angles quoted for the Cluster detectors are between the beam direction and the axis of the central crystal, and for the MINIBALL detectors between the beam and the central axis of the triple cryostat.

importance of efficiency to energy resolution to achieve the physics goals of a particular experiment. A summary of the detectors and their positions is given in Table 1.

To allow access to the target position, maintenance of the spectrometer and the option of running non-RISING experiments with the detectors still in the experimental area, the array splits perpendicular to the beam direction, moving 1.4 m on one side and 3.2 m on the other side.

In the second phase, the existing three rings of Cluster detectors are maintained and the MINIBALL detectors [40] are added in two rings with the axis of centre of the triple cryostats at 51.3° and 86.0°. Each ring can consist of up to five detectors, although only a total of eight detectors will be available. Again a range of target to detector distances is permitted. These detectors are a further development of those used in the Cluster detectors. Each MINIBALL detector comprises three encapsulated Ge crystals, the same size as the Cluster capsules, mounted in one cryostat. Each of these capsules is electronically segmented six ways on its outer surface. The signals from each segment are read out independently and passed to a digital electronics system. The digital electronics is then used to determine the energy, time of interaction and, by complex pulse shape analysis, the position of interaction in the crystal. Information on the position of the main interaction in the crystal, supposed to be the first interaction, is extremely useful in these fast beam experiments since the correspondingly improved Doppler correction allows the detector to be placed significantly closer to the target. This increases the efficiency while maintaining good resolution. If a position resolution determination of 5 mm is assumed, a minimum distance smaller than the beam pipe diameter (130 mm) for a detector angle of 90° is derived for 1% energy resolution at $\beta = 0.43$.

However, the minimum distance is determined by the mechanical constraints of the beam pipe and target chamber (relaxing the position resolution requirement). There is an additional constraint imposed by the isolated hit probability and the intense atomic background. As discussed in Section 2.2 the dominant background from bremsstrahlung scales with the charge of projectile and target. For the worst case, corresponding to a ^{238}U beam incident on a ^{208}Pb target, the closest Ge detectors may be placed 400 mm distance from the target.

Table 2
Estimated performance of an array with Ge detectors at the closest position and at a position optimised for energy resolution considering the highest background from atomic radiation

Ring	Distance (mm)	Energy resolution (%)	Efficiency (%)
1	700	1.00	1.00
2	700	1.82	0.91
3	700	1.93	0.89
Total Cluster		1.56	2.81
4	180	0.70	2.75
	227	0.57	0.46
5	180	0.68	1.01
	232	0.56	0.32
Total MINIBALL		0.67	4.55
Total array		1.01	7.35
1	700	1.00	1.00
2	1295	1.01	0.28
3	1372	1.01	0.24
Total Cluster		1.00	1.52
4	400	0.36	0.82
5	400	0.37	0.36
Total MINIBALL		0.36	1.18
Total array		0.73	2.70

The given efficiencies include the Lorentz boost.

Table 2 shows the calculated performance of RISING assuming a 1.3 MeV γ ray emitted from a nucleus moving at $\beta = 0.43$. In these calculations the velocity spread in the target and the recoil cone were ignored. The total energy resolution is a weighted average of the energy resolution scaled by the efficiency.

All experiments so far were performed with the Cluster detectors in their closest position (700 mm). To reduce the contribution from the atomic background radiation, each Cluster detector was surrounded on the side by the lead shield of 2 mm thickness, and had in the front side a combination of Pb, Sn and Al absorbers of 5 mm thickness. The efficiency was determined experimentally with standard γ-ray sources. A comparison with corresponding simulation calculations revealed a very good agreement. Multiplying with the appropriate Lorentz factor results in 3% efficiency at 100 A MeV for 1.3 MeV γ ray. The preliminary energy resolution ranging from 1.2% to 1.5% is in agreement with the calculated value.

6. High-energy γ-ray detection with the HECTOR array

In order to have the possibility of measuring low and high energy γ rays with comparable efficiency, eight large-volume BaF_2 scintillators (part of the HECTOR array) are placed in the RISING set-up. These detectors have a good time resolution and high detection efficiency, complementing the Ge-Cluster detectors. The sub-nanosecond time resolution means that one can use the time information to identify sources of various background components. In addition, these detectors can be used to measure low-energy transitions when they correspond to well separated lines in the spectra resulting in an increase of the overall efficiency of the γ-ray detection system.

6.1. HECTOR array for experiments at relativistic energies

The HECTOR array consists of eight large scintillating crystals of BaF_2, 145 mm in diameter and 175 mm in length [43,44]. The crystals are tapered for half of the length in a hexagonal shape and have a cylindrical shape for the second half. Each crystal is coupled to a single fast photo-multiplier tube (EMI 9823QA, 125 mm in diameter) with a quartz window, selected for its stability in terms of counting rate and connected to an active voltage divider. Each BaF_2 detector works at an operating voltage set between −1500 and −1800 V to maximise the linearity of its response with respect of the incident energy. For the same purpose, the energy signal is taken from the 10th dynode of the photo-multiplier. Due to the very fast scintillation light of BaF_2 material, each detector has a sub-nanosecond intrinsic time resolution. The energy resolution is of the order of 10% for the 1173 and 1332 keV lines of ^{60}Co.

The gain fluctuations of each detector are monitored by a LED system that produces three light pulses of different intensity corresponding to three different energies detected in the crystal, spread over the range of interest of the experiment. The light pulses can be triggered either internally or externally by a NIM signal [45]. The internal radiation arising from radium contaminations in BaF_2 crystals is used to monitor the performance of the detectors.

In the RISING set-up, the BaF_2-HECTOR detectors are placed at 350 mm from the target at a backward angle of 142°. It is also possible to place two detectors at 90° without interfering with the Ge-Cluster detectors or with MINIBALL Ge detectors. This geometry represents a compromise to get the maximum solid angle, with a minimum

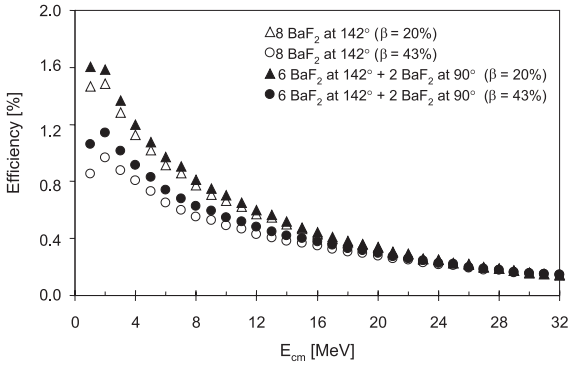

Fig. 10. Simulated HECTOR array efficiency as a function of γ-ray energy in the centre of mass frame.

Doppler broadening effect. To reduce the contribution from the atomic background radiation, each crystal is surrounded on the side by a lead shield of 6 mm thickness, and has on the front side selectable Pb-absorbers of 1, 3 or 6 mm thickness.

The performance of the BaF_2-HECTOR detectors in the RISING set-up and for the measurement of γ rays from relativistic beams has been simulated using the GEANT 3.21 programme [46]. Fig. 10 shows the absolute full-energy peak efficiency for the BaF_2 detectors placed at 350 mm at 142° or 90° and assuming a source velocity of $\beta = 0.2$ and 0.43.

6.2. Background investigation in the commissioning phase

In addition to the primary role of measuring high-energy γ rays emitted from the giant dipole resonance, the eight BaF_2 detectors have been shown to be very useful for the investigation of sources of disturbing background radiation in the RISING experiments.

Fig. 11 shows the time spectra measured with the 142° BaF_2-detector as obtained with a ^{84}Kr beam at 113 A MeV on an Au target and for an empty target frame. The spectra show a rather large contribution from background radiation (the broad distribution peaked at −5 ns). From the value of the centroid position of the broad

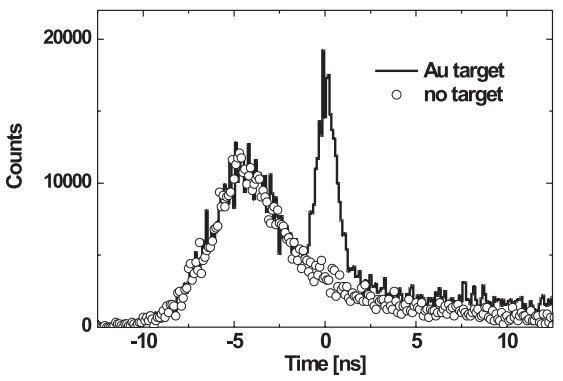

Fig. 11. Time spectra measured with a BaF_2 detector with respect to start signals from the plastic scintillator SCI2, using the relativistic ^{84}Kr beam and an Au-target (solid line), or an empty target frame (open circles).

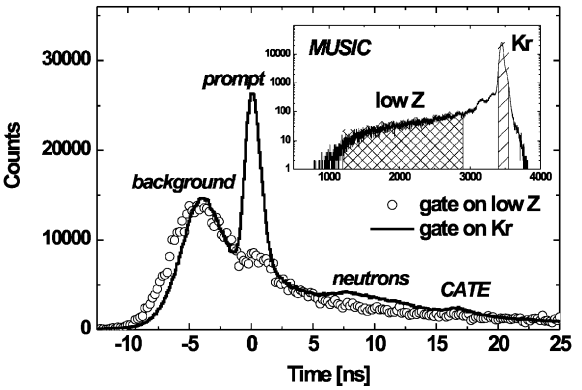

Fig. 12. Time spectra gated by the energy deposited in the MUSIC chamber (see inset), one gate corresponds to the low-Z fragments (open circles) and the other gate to the Z of the primary Kr beam (solid line).

structure it is deduced that this background radiation is originating from decays occurring at a distance of 1–4 m upstream from the target. The prompt radiation from the target gives rise to the narrow peak at $t = 0$.

Fig. 12 shows two time spectra gated by different values of the energy deposited in the MUSIC detector. The spectrum gated on the low-Z fragments has a shape very similar to that measured with the target frame only (see Fig. 12) and therefore it contains predominantly the background contribution. In contrast, the spectrum gated by the Z value of the ^{84}Kr beam clearly shows the prompt peak associated with events from the target. The background radiation, preceding the prompt peak from the target, still remains indicating that it is related to fragmentation reactions occurring behind the MUSIC chamber. In addition, different components of the radiation detected by the BaF_2 detector are seen. Delayed radiation and neutrons emitted from the target (7–12 ns after the prompt peak) and the γ radiation from reactions induced by the Kr beam hitting the CATE detector (17 ns after the prompt radiation), can be identified. Following this observation, a Pb absorber wall has been built to reduce the upstream background which cannot be separated by time conditions in the Ge detectors due to their limited time resolution.

7. Data acquisition and control system

As described in previous sections, RISING is a combination of three independent detector systems, the EUROBALL Ge-Cluster detectors, the HECTOR array and the FRS detectors including the CATE array. Each of these systems has an individual data acquisition systems (DAQ) producing independent events. To assemble them in common events, a time-stamping technique for event synchronisation, was developed in the framework of the GSI standard DAQ system, MBS [47]. Each sub-system is equipped with a newly developed VME time stamping module, TITRIS [48]. It produces a single-hit 48-bit time stamp with the least significant bit being 20 ns. As the hardware set-up is identical in all branches one TITRIS module is arbitrarily chosen to be a master, while all the others are slaves. All of them are connected in a line via a synchronisation bus, the length of which can exceed 100 m. The master module sends regularly synchronisation pulses to all slave modules and in this way keeps all modules on the same time base. Within this procedure, the signal cable delay of the calibration pulses is automatically taken into account by the slave modules. Tests and in-beam measurements revealed a precision better than 20 ns (RMS) for the complete timing system. Within the TITRIS module, the special daisy-chain readout is available, which is mandatory for the EUROBALL VXI system. The design of the time stamping system allows for the integration of up to 16 TITRIS modules in a system. Thanks to this new approach it is possible to keep most of the original components of the RISING sub-systems in operation. They still run independently and are fully operational DAQ systems with individual trigger sources and produce their local dead time for the readout. In addition, it is also possible to feed identical triggers into all sub-system and to combine their local dead times, as it was done for the RISING set-up. Upon receipt of each accepted trigger, the digitisers are read out and the event data are sent via a TCP socket to an event builder. The time-stamping module gets a signal

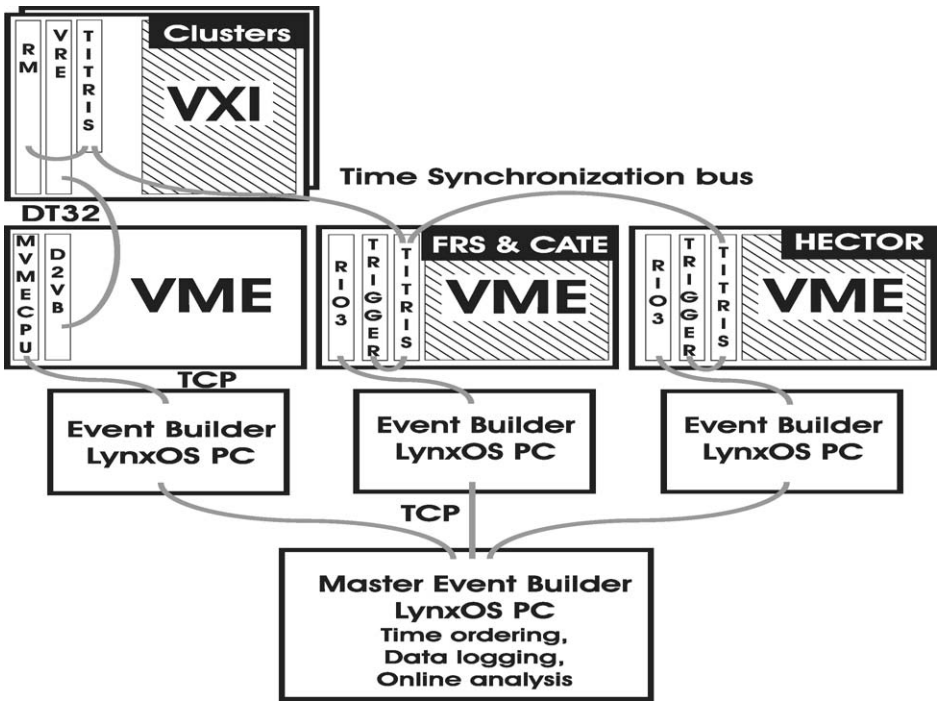

Fig. 13. Block diagram of the RISING data acquisition system.

from the Master Trigger Output signal for each accepted trigger. The time difference of the time stamps from the same trigger amounts to about 3 μs and is caused by various signal delay times of the VXI trigger card and the Master Trigger Output of the VME trigger module. This constant time offset must be taken into account for the time matching of events from different sub-systems. A schematic diagram of the RISING DAQ system is presented in Fig. 13.

The Cluster detector signals are processed and digitised by the VXI Ge-Cluster cards providing 4 and 20 MeV energy ranges and γ-ray time with respect to the VXI trigger. The cards are read out by the VXI Readout Engine (VRE) and then sent via the DT32 bus (10 MHz, 32-bit differential ECL) to a VME processor [49]. Up to this stage the procedure is identical to previous EUROBALL experiments [50]. The VXI modules and DAQ are controlled by the MIDAS software package [51]. On the VME processor a new programme developed for RISING sends event data in large data blocks via TCP sockets to an MBS event-builder PC. This event-builder receives the data, converts it into the MBS data format and provides it for further processing like data logging, online monitoring and most importantly as a data source for the RISING master event-builder described below. The DAQ system for FRS/CATE and HECTOR are structurally identical MBS systems. A VME crate contains a RIO3 readout processor, the GSI trigger module, the TITRIS time stamping module and digitisers, QDC, ADC, TDC, scaler and pattern unit. The energy and time signals from the BaF_2 detectors were collected for the HECTOR DAQ. For the fast component, a dedicated signal shaping and stretching module was developed to adopt the timing signal to the Ge branch. In order to set up and calibrate the BaF_2 array, a special data acquisition system, based on K-Max 7.2 [52] was employed.

The collecting and sorting of the data from all sub-systems is made by the RISING master event-builder running with an independent MBS system. For this purpose a new MBS programme has been developed. It has to fulfil three main tasks:

(1) Connect (and disconnect) rapidly to the sub-systems data output stream via TCP sockets. This allows for easy partitioning of the DAQ system, i.e. during set up phases.
(2) Sort all events from the connected systems according to their time stamps in ascending order into a single data output stream.
(3) Format all events into output buffers for data logging and online monitoring purposes.

It is the task of the data analysis, not the DAQ system, to select from the time-sorted event stream those which have to be combined into a real "physics" events. This allows the flexibility of using different criteria to compose events from identical data sets.

The basic trigger signal is derived from the SCI2 (see Section 3) providing a fast NIM signal, useful in defining local triggers and establishing the time reference. Two kinds of physics triggers are implemented with the help of the SCI2 signal:

(1) SCI2 and at least one γ ray in any Cluster detector in coincidence form a physics trigger, which is fed simultaneously to the Cluster detector—and the FRS/CATE DAQ system.
(2) SCI2 in coincidence with at least a single γ ray in the HECTOR array. This trigger initiates the readout of FRS/CATE and HECTOR.

In addition, a γ-ray singles trigger for calibration and control purposes is foreseen. A second type of a trigger is associated with generation of control LED pulses used to monitor the stability of the detector gains.

The on-line analysis of the combined RISING data was performed using the GO4 package developed at GSI [53]. An object-oriented programme picked up a portion of the data output stream from the MBS master event builder. Subsequently, it produced raw histograms and allowed for merging time sorted sub-events into complete physical events. Various conditions on the histograms could be set and combined in an unrestricted way using a graphical user interface [54], which also facilitated visualisation of the histograms. Among other plots, two-dimensional synchronisation matrices of control signals originating from different MBS branches were dis-

Table 3
Summary of experimental details of the first RISING measurements including the nucleus of interest, primary and secondary beams, secondary targets, excitation methods and γ-ray transitions of interest

Nucleus of interest	^{84}Kr	^{56}Cr	^{53}Ni	^{108}Sn
Primary beam (A MeV)	^{84}Kr	^{86}Kr	^{58}Ni	^{124}Xe
(SIS energy)	165	419	600	700
Secondary beam (A MeV)	—	^{56}Cr	^{55}Ni	^{108}Sn
(energy at target)	113	136	171	142
Secondary target	^{197}Au	^{197}Au	^{9}Be	^{197}Au
Thickness (g/cm^2)	0.4	1.0	0.7	0.4
Experimental method	Coul. ex.	Coul. ex.	Two-step. frag.	Coul. ex.
γ ray of interest (keV)	882	1006	Unknown	1206
$I_i^\pi \rightarrow I_f^\pi$	$2^+ \rightarrow 0^+$	$2^+ \rightarrow 0^+$		$2^+ \rightarrow 0^+$

played. Calibrated and Doppler-corrected γ-ray spectra, gated by the tracking detectors, were available on-line.

8. First experiments and data analysis

Four experiments have been performed with the RISING set-up so far. Table 3 summarises experimental details of the measurements including the nucleus of interest, primary and secondary beams, secondary target, experimental method and the γ-ray transition of interest. In all cases γ rays depopulating excited states were measured by the Ge-Cluster and BaF_2-HECTOR arrays. Preliminary results of the still on-going data analysis will be presented to illustrate the performance of the set-up.

In the first experiment, a primary beam of ^{84}Kr was impinging on a ^{197}Au target mounted in the final focal plane of the FRS in order to investigate the feasibility of Coulomb excitation measurements under the best beam conditions by measuring the $2^+ \rightarrow 0^+$ γ transition in ^{84}Kr and to study the particle–γ angular correlation at relativistic energies. Two relativistic Coulomb excitation experiments with secondary beams were performed to measure B(E2) values of transitions, depopulating the first 2^+ state in radioactive neutron-rich ^{56}Cr and neutron-deficient ^{108}Sn. In the case of ^{108}Sn, a thinner ^{197}Au target and higher energy of the secondary beam than in the case of ^{56}Cr were chosen because of the expected short lifetime (∼ 0.4 ps) of the first 2^+ state of ^{108}Sn. Thus, the fraction of γ rays from decays in the target, causing large Doppler-shift uncertainties, as discussed in Section 5.1, is reduced.

A two-step fragmentation method was applied to identify the first excited states in ^{53}Ni. The goal of the measurement was to study the mirror symmetry between ^{53}Ni and ^{53}Mn. A secondary beam of ^{55}Ni was produced by fragmentation of a ^{58}Ni primary beam on a Be target, and was impinging on a secondary beryllium target mounted at the final focal plane of the FRS. The reaction fragments were detected by CATE using the ΔE–E correlation.

Data analysis was performed by software based on GO4 [53] and ROOT [55], developed for off-line analysis. The examples shown below are the first results of the RISING experiments on ^{84}Kr, ^{56}Cr and ^{53}Ni.

The selected particles, reaching the secondary target were identified in terms of A/Q and Z by TOF and MUSIC, respectively, as described in Section 3. Out-going particles after the target were identified and selected by CATE using ΔE–E correlations. Since the mass analysis of CATE is still in progress, only different elements can be selected at present. γ rays within a time range of ±25 ns were selected with a further requirement of multiplicity $M_\gamma = 1$ for $E_\gamma \geqslant 500$ keV (in the laboratory frame). In- and out-going particles were tracked by the two Multi-Wire chambers before the target and by CATE behind the target.

The vertex on the target, the scattering angle between an in- and an out-going particle and the angle between an out-going particle and a γ ray were calculated event-by-event. A range of scattering angles was selected in order to enhance the Coulomb excitation events. The calculated angle between an out-going particle and a γ ray was used for Doppler correction. A velocity factor, β_t, behind the target, which is used for Doppler correction, was calculated event-by-event by using the TOF measurement with the two plastic scintillators together with the calculated energy loss in the target.

Since in the ^{84}Kr experiment the primary beam directly impinged on a gold target, selection of the in-coming projectile was not necessary and a fixed $\beta = 0.396$ was used for the Doppler correction. Out-going particles with $Z = 36$ were selected by CATE. A conservatively chosen range of scattering angles between 0.7° and 1.5° was demanded. Fig. 14(b) shows a Doppler-corrected γ-ray spectrum under the above conditions. The

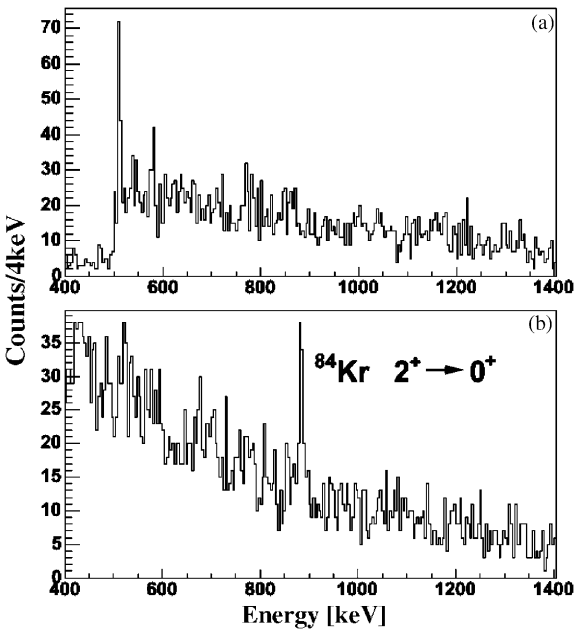

Fig. 14. Gamma-ray spectra for 113 A MeV ^{84}Kr projectile Coulomb excitation on a 0.4 g/cm^2 thick Au target, (a) without and (b) with Doppler correction. The $2^+ \rightarrow 0^+$ transition at 882 keV is marked.

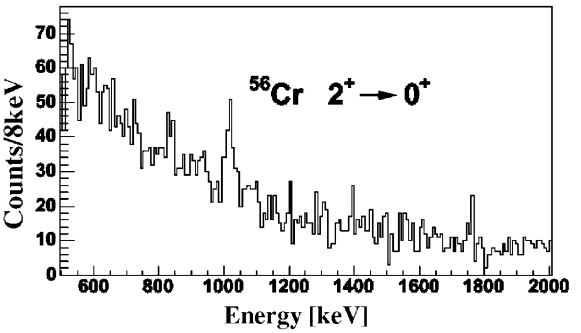

Fig. 15. Doppler-corrected γ-ray spectrum of ^{56}Cr Coulomb excitation at 136 A MeV on a 1.0 g/cm^2 gold target.

882 keV ($2^+ \rightarrow 0^+$) transition of ^{84}Kr is clearly visible. No background subtraction was applied. The FWHM and the significance of the peak are 1.5% and 8σ, respectively. For comparison, the same spectrum without Doppler correction is displayed in Fig. 14(a). Here, the γ-ray intensity corresponding to the ($2^+ \rightarrow 0^+$) transition is distributed between 1100 and 1400 keV leaving no indication of a peak.

For the analysis of the ^{56}Cr data similar method was applied. Out-going particles with $Z = 24$ and a scattering angle between 0.5° and 3.5° were selected by CATE to enhance Coulomb excitation events. The velocity, β_t, was determined event-by-event with the TOF measurements and corrected for energy loss in the target. In Fig. 15, the Doppler-corrected γ-ray spectrum under the above conditions is shown. The $2_1^+ \rightarrow 0^+$ transition at 1006 keV is clearly observed.

For the ^{53}Ni data only very preliminary results of the analysis performed during the experiment are currently available. As no information on tracking and TOF was used for the event reconstruction, the angle of Ge-detectors with respect to the target centre was used for the Doppler-correction with a fixed $\beta_t = 0.45$. The selection of scattering angles was not done. In Fig. 16, Doppler-corrected γ-ray spectra are shown for different element selection by CATE, (a) Co, (b) Fe, and (c) Cr. For these spectra only 10% of the data were analysed. In Fig. 16(a), the known γ-transitions ($2^+ \rightarrow 1^+$) at 509 keV and ($1^+ \rightarrow 0^+$) at 937 keV in ^{54}Co are indicated. In Fig. 16(b), the

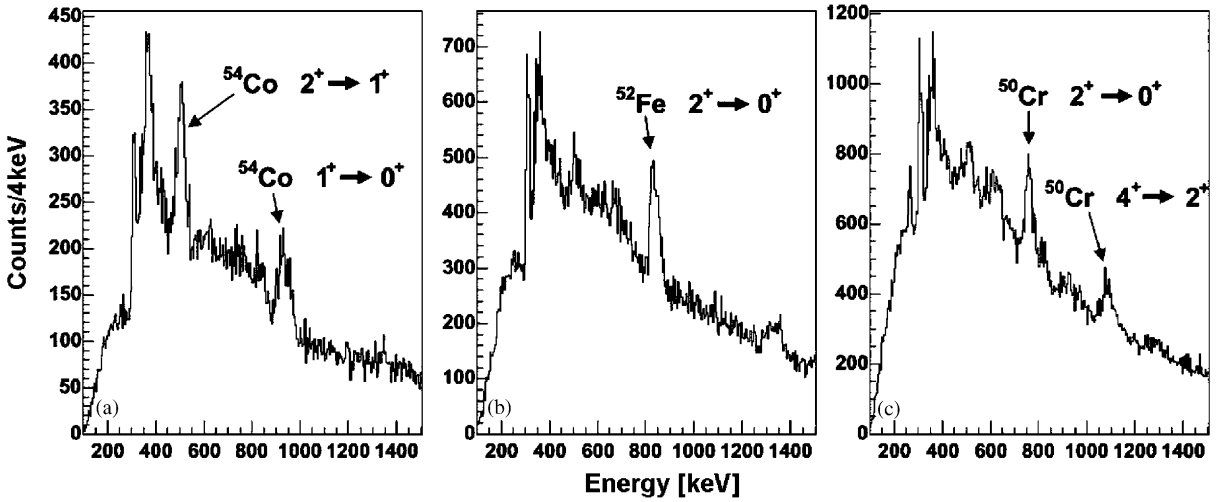

Fig. 16. Gamma-ray spectra of the fragmentation reaction ^{55}Ni on ^{9}Be with selection on different elements: (a) Co, (b) Fe, and (c) Cr.

($2^+ \rightarrow 0^+$) 849 keV transition of ^{52}Fe is shown, and in Fig. 16(c) the ($2^+ \rightarrow 0^+$) and ($4^+ \rightarrow 2^+$) transitions of ^{50}Cr at 783 and 1098 keV, respectively, are present, demonstrating that fragmentation reactions populate states with spins beyond $2\hbar$. Additional peak structures in all three spectra are due to the decay of higher lying states of the selected isotopes and transitions in other isotopes since no mass selection was applied. The γ-ray energies in Fig.16 are slightly shifted as compared to the literature values and the peaks are broader than expected. This results from the absence of tracking and β measurement in the on-line analysis. The event-by-event analysis which is now in progress will significantly improve the final result.

9. Summary and conclusion

The RISING set-up allows for high-resolution γ-ray spectroscopy experiments employing beams of short-lived isotopes at 100 A MeV energy from the SIS/FRS facility at GSI. It comprises heavy-ion tracking detectors for incoming beam nuclei impinging on a secondary target, the CATE detector for outgoing heavy ions and the EUROBALL Ge-Cluster detector and BaF_2-HECTOR detector arrays for γ-ray detection. A new data acquisition system with independent subsystems linked by time stamps was employed for the first time at GSI to connect three data branches.

The set of particle detectors is capable of uniquely determining the mass and charge of each beam nucleus with the necessary precision. In addition, they allow the measurement of the velocity and direction of the fast-moving nucleus, information necessary to perform the Doppler correction of the measured γ-ray energy. The first phase of the Cluster array has a full-energy efficiency of 3% with 1.2–1.5% energy resolution at 100 A MeV. The novel position-sensitive ΔE–E calorimeter, CATE, enables an accurate scattering angle determination, limited only by target angular straggling. The charge identification is unique and a mass identification with a resolution of $\Delta A/A \geqslant 0.5\%$ is expected, depending on further ongoing complex analysis steps. The excellent time resolution of the HECTOR array has been used to identify background sources, which were reduced during commissioning.

The first Coulomb excitation and secondary fragmentation experiments with RISING demonstrated that the set-up fulfils all requirements and provides a new powerful instrument for high-resolution in-beam γ spectroscopy at relativistic energies.

Acknowledgements

The collaboration would like to thank the EUROBALL Owners Committee, the MINIBALL Collaboration and the HECTOR collaboration for making the detectors available for the RISING campaigns at GSI. J.J., P.R. and N.W. acknowledge support of the BMBF under grant 06OK-167. H.H. and A.B. acknowledge support of the BMBF under grant 06BN-109. K.-H.S. and J.L. acknowledge support of the BMBF under grant 06BN-911. The Swedish coauthors acknowledge the Swedish Research Council. The Polish coauthors acknowledge the Polish State Committee for Scientific Research (KBN Grant No. 2P03B 118 22).

References

[1] H. Geissel, et al., Nucl. Instr. and Meth. B 70 (1992) 286.
[2] J.F. Ziegler, J.B. Biersack, U. Littmark, The Stopping and Range of Ions in Solids, vol.1, Pergamon Press, Oxford, 1985.
[3] http://www-linux.gsi.de/weick/atima/.
[4] R. Anhold, S.A. Andriamonje, E. Morenzoni, C.H. Stoller, J.D. Molitoris, W.E. Meyerhof, H. Bowman, J.-S. Xu, J.O. Rasmussen, D.H.H. Hoffmann, Phys. Rev. Lett. 53 (1984) 234.
[5] R. Anhold, et al., Phys. Rev. A 33 (1986) 2270.
[6] R. Holzmann, K. Grimm, R. Kulessa, E. Wajda, H. Xie, M. Zinser, the LAND Collaboration, GSI Annual Report, 1992, p. 48.
[7] T. Glasmacher, Annu. Rev. Nucl. Part. Sci. 48 (1998) 1.
[8] W.W. Wilcke, J.R. Birkelund, H.J. Wollersheim, A.D. Hoover, J.R. Huizenga, W.U. Schröder, L.E. Tubbs, At. Data Nucl. Data Tables 25 (1980) 391.
[9] J.D. Jackson, Classical Electrodynamics, Wiley, New York, 1974, p. 620.
[10] F. Azaiez, et al., Nuclear Structure 98, Gatlinburg, TN, AIP, Conference Proceedings, vol. 481, 1998, p. 243.
[11] S. Wan, et al., Eur. Phys. J. A 6 (1999) 167.
[12] K. Yoneda, et al., Phys. Lett. B 499 (2001) 233.
[13] J.-J. Gaimard, K.-H. Schmidt, Nucl. Phys. A 531 (1991) 709.
[14] M. de Jong, A.V. Ignatyuk, K.-H. Schmidt, Nucl. Phys. A 613 (1997) 435.
[15] K. Sümmerer, B. Blank, Phys. Rev. C 61 (2000) 034607 and references therein.
[16] K. Sümmerer, B. Blank, EPAX version 2.1 http://www-w2k.gsi.de/hellstr/asp/gsi/epaxv21m.asp.
[17] T. Enqvist, et al., Nucl. Phys. A 658 (1999) 47.
[18] J. Benlliure, K.-H. Schmidt, D. Cortina-Gil, T. Enqvist, F. Farget, A. Heinz, A.R. Junghans, J. Pereira, J. Taieb, Nucl. Phys. A 660 (1999) 87.
[19] C. Engelmann, et al., Z. Phys. A 352 (1995) 351.
[20] M. Bernas, et al., Phys. Lett. B 331 (1994) 19.
[21] M. Bernas, et al., Phys. Lett. B 415 (1997) 111.
[22] C. Donzaud, et al., Eur. Phys. J. A 1 (1998) 407.
[23] W. Schwab, et al., Eur. Phys. J. A 2 (1998) 179.
[24] J. Benlliure, et al., Eur. Phys. J. A 2 (1998) 193.
[25] H.J. Wollersheim, www-aix.gsi.de/~wolle/ISOMER/fission_cross.pdf.
[26] N. Iwasa, et al., Nucl. Instr. and Meth. B 126 (1997) 284.
[27] O. Tarasov, D. Bazin, Nucl. Instr. and Meth. B 204 (2003) 174; The LISE code web sites: http://groups.nscl.msu.edu/lise and http://dnr080.jinr.ru/lise.
[28] H. Stelzer, Nucl. Instr. and Meth. A 310 (1991) 103.
[29] R. Schneider, A. Stolz, Technical Manual Ionisation Chamber MUSIC80, 2000.
[30] N. Le Neindre, et al., Nucl. Instr. and Meth. A 490 (2002) 251.
[31] R. Lozeva, et al., to be published.
[32] T. Doke, J. Kikuchi, H. Yamagichi, S. Yamaguchi, K. Yamamura, Nucl. Instr. and Meth. A 261 (1987) 605.
[33] U. Bonnes, J. Foh, private communication.
[34] P. Doornenbal, Diploma Thesis, University of Frankfurt, Germany, 2003.
[35] R. Lozeva, et al., Nucl. Instr. and Meth. B 204 (2003) 678.
[36] A. Pullia, R. Bassini, C. Boiano, S. Brambilla, IEEE Trans. Nucl. Sci. NS-48 (3) (2001) 530.
[37] D. Pelte, D. Schwalm, In-beam Gamma-ray Spectroscopy with Heavy Ions, North-Holland, Amsterdam, 1982.
[38] D. Schwalm, A. Bamberger, P.G. Bizzeti, B. Povh, G.A.P. Engelbertink, J.W. Olness, E.K. Warburton, Nucl. Phys. A 192 (1972) 449.
[39] J. Simpson, Z. Phys. A 358 (1997) 139; Achievements with the EUROBALL spectrometer, in: W. Korten, S. Lunardi (Eds.), Scientific and Technical Report 1997–2003, 2003, http://www-dapnia.cea.fr/Sphn/Deformes/EB/eb-report-final.pdf.
[40] J. Eberth, et al., Prog. Part. Nucl. Phys. 46 (2001) 389.
[41] J. Eberth, et al., Nucl. Instr. and Meth. A 369 (1996) 135.
[42] M. Wilhelm, et al., Nucl. Instr. and Meth. A 381 (1996) 462.
[43] A. Maj, et al., Nucl. Phys. A 571 (1994) 185.
[44] F. Camera, Ph.D Thesis, University of Milano, Italy, 1992.
[45] A. Boiano, et al., to be published.
[46] CERN Geneva, GEANT—Detector Description and Simulation Tool [online]. pp. 1–430. Available: http://wwwinfo.cern.ch/asd/geant/geantall.ps.gz.
[47] H.G. Essel, J. Hoffmann, N. Kurz, R.S. Mayer, W. Ott, D. Schall, IEEE Trans. Nucl. Sci. NS-43 (1) (1996) 132; H.G. Essel, N. Kurz, IEEE Trans. Nucl. Sci. NS-47 (2) (2000) 337.
[48] J. Hoffmann, N. Kurz, GSI Scientific Report, 2002, p. 224.
[49] I. Lazarus, P. Coleman-Smith, N. Karkour, G.M. McPherson, A. Richard, C. Ring, IEEE Trans. Nucl. Sci. NS-39 (1992) 1352;

I. Lazarus, P.J. Coleman-Smith, IEEE Trans. Nucl. Sci. NS-42 (1995) 891;
I. Lazarus, P. Coleman-Smith, J. Thornhill, G. Bosson, N. Karkour, A. Richard, Z. Zojceski, C. Ring, IEEE Trans. Nucl. Sci. NS-42 (1995) 2288;
M.M. Aleonard, et al., IEEE Trans. Nucl. Sci. NS-39 (1992) 892;
J. Alexander, F.A. Beck, C. Ender, I. Lazarus, G.M. McPherson, E.C.G. Owen, J. Pauxe, A. Richard, C. Ring, IEEE Trans. Nucl. Sci. NS-39 (1992) 886.

[50] G. Maron, V. Pucknell, A data acquisition system for EUROBALL III, EDOC306, http://npg.dl.ac.uk/documents/edoc306/.
[51] V.F.E. Pucknell, The MIDAS Multi Instance Data Acquisition System, http://npg.dl.ac.uk/MIDAS.
[52] KMAX—Sparrow Corporation, 1901 Poppy Lane Port Orange, FL 32128, USA.
[53] http://www-w2k.gsi.de/go4/.
[54] J. Grębosz, private communication.
[55] http://root.cern.ch/.